Journal Name

ARTICLE TYPE

Cite this: DOI: 00.0000/xxxxxxxxxx

Impact of dehydration and mechanical amorphization on the magnetic properties of Ni(II)-MOF-74†

Senada Muratović,[a] Bahar Karadeniz,[a] Tomislav Stolar,[a] Stipe Lukin,[a] Ivan Halasz,[a] Mirta Herak,[b] Gregor Mali,[c] Yulia Krupskaya,[d] Vladislav Kataev,[d] Dijana Žilić*[a] and Krunoslav Užarević*[a]

Received Date
Accepted Date

DOI: 00.0000/xxxxxxxxxx

Mechanically responsive metal-organic frameworks (MOFs) came very recently into the spotlight of material science for their unique properties and potential new fields of application. We present here a clarification of the magnetic properties of prototypical magnetic MOF-74 material, Ni(II)-MOF-74, using magnetization measurements, X-band electron spin resonance (ESR), multi-frequency high-field ESR (HF-ESR), and theoretical model. It was established that the guests populating the honeycomb channels have little influence on the magnetism of Ni-MOF-74, whereas magnetic properties depend strongly on the degree of the internal ordering in the structure. Amorphous material (*am*-Ni-MOF-74), which can be readily prepared by the mechanochemical treatment of dehydrated Ni-MOF-74 (*deh*-Ni-MOF-74), as shown by *in situ* monitoring methods, displays significantly lower bulk magnetization compared to Ni-MOF-74 and *deh*-Ni-MOF-74. This decline in magnetization is established to be a consequence of the spin-crossover from high-spin to a low-spin state of nickel(II) ions. The observed spin-crossover was rationalized by an insight into the changes of the nickel coordination sphere during the amorphization, which was provided by solid-state nuclear magnetic resonance (NMR) and infrared (IR) spectroscopy. Additionally, it was found that *am*-Ni-MOF-74 behaves differently than its zinc analogue when exposed to vapors or liquid-additives in the milling process, indicating that the nature of the metal node plays a substantial role in the mechanical properties of this modular family of MOF materials.

1 Introduction

Metal-organic frameworks (MOFs) [1–3] are subject of intensive research due to their promising applications in storage, [4,5] separation, [6–8] light- and water harvesting, [9–11] sensing, [12,13] destruction of warfare agents, [14,15] and catalysis, [16–18] to name just a few. Most of their properties arise from a well-ordered, porous crystalline frameworks comprised of metal nodes and organic linkers, which can be tuned and even designed to suit a particular application. The most interesting properties of these materials, however, are related to their structural flexibility. It was found only recently that particular MOFs are stimuli-responsive, meaning that they can adjust their structure, reversibly or irreversibly, in response to external chemical or physical stimuli, such as interaction with guests, gas pressure or pH change, mechanical stress, light, temperature, and others. [19]

Mechanically-responsive MOFs came into a spotlight due to their flexibility and unique properties among inorganic compounds [20–22] including anomalous and anisotropic mechanical properties, like negative linear compressibility or negative Poisson ratio. A lot of interest, however, both from fundamental and technological points, [23] is now in MOFs which undertake large-scale transformations under mechanical action, such as phase transitions or amorphization. Amorphous MOFs, despite contradicting to original postulates of MOF chemistry which are focused exclusively on highly-ordered and crystalline products, have already found new applications in sensing, reversible and irreversible storage of harmful compounds, tunable drug release, and even in the synthesis of MOF glasses and glassy composites. [24–26] The field is only starting to emerge, and there are still very few studies available showing how amorphization reflects on physical properties like photoluminescence, magnetism, conductivity, and similar, which will present an obstacle in expanding the applicability

[a] *Ruđer Bošković Institute, Bijenička cesta 54, 10000 Zagreb, Croatia. Email: dijana.zilic@irb.hr, krunoslav.uzarevic@irb.hr*
[b] *Institute of Physics, Bijenička cesta 46, 10000 Zagreb, Croatia.*
[c] *National Institute of Chemistry, Hajdrihova 19, SI-1001 Ljubljana, Slovenia.*
[d] *Leibniz IFW Dresden, Helmholtzstrasse 20, D-01069 Dresden, Germany.*

† Electronic Supplementary Information (ESI) available: Experimental, Simulation of ESR spectra, Additional PXRD, SEM, magnetization, ESR, NMR, TGA and Raman figures. See DOI: 00.0000/00000000.

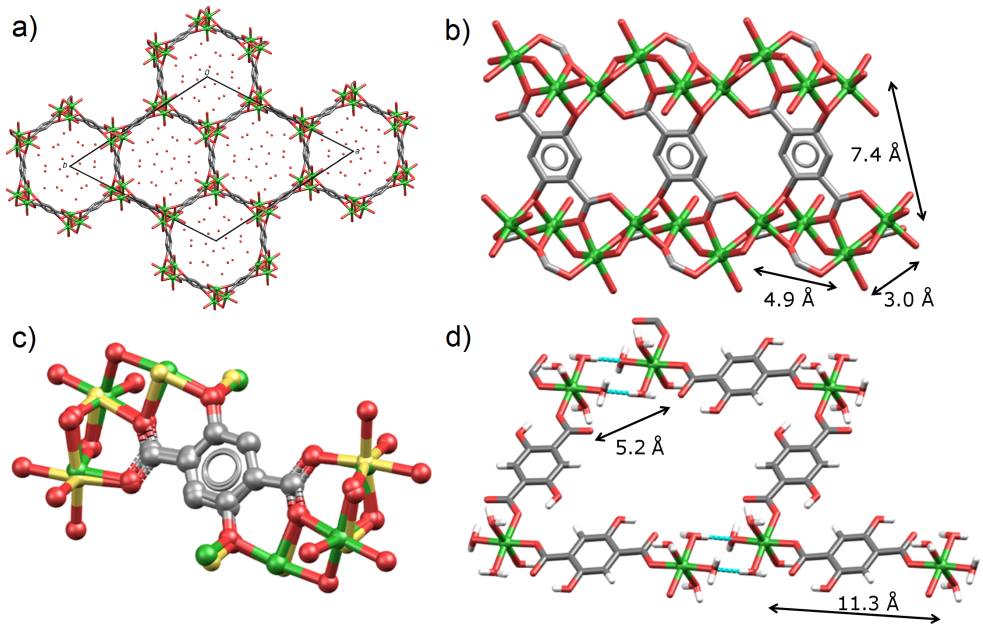

Fig. 1 a) Honeycomb channels in the crystal structure of Ni-MOF-74. b) Cross-section of wall structure in Ni-MOF-74 along c-axis (Ni–green, O–red, C–gray) showing two helical nickel(II) chains; the nearest-neighbours of nickels are separated around 3.0 Å, next-nearest neighbors around 4.9 Å, while the closest distance between nickels in different chains is around 7.4 Å. c) Overlay of Ni-MOF-74 and Zn-MOF-74 structures (Zn–yellow). d) Two chains in Ni-INT compound are stabilized by O−H···O ring-like hydrogen bonds (blue stippled lines). The shortest distance between the nickels in the chain of Ni-INT is around 11.3 Å, while the shortest distance between the nickel centers in two different chains (5.2 Å) is over an O−H···O hydrogen-bonded ring. The crystalline water molecules are omitted for clarity sake.

of amorphous MOFs to other relevant areas of material science.[27]

MOF-74 family, also known as CPO-27-M,[28–30] attracted a lot of attention due to their modularity, thermal and chemical stability, open metal sites, and well-defined large channels (diameter *ca.* 12-15 Å) in their honeycomb structure. MOF-74 materials are widely studied for storage and catalytic applications related to open metal sites, but also for their magnetic properties arising from complex connectivity of metal cations organized in one-dimensional (1D) oxo-bridged helical chains, placed on the corners of hexagonal channels that mutually interact through organic bridges in lateral directions (Fig. 1a and b).[31] One of the most interesting magnetic MOFs is Ni(II)-MOF-74 (Ni-MOF-74).[32,33] However, the magnetic properties of Ni-MOF-74 are still not clear since the available computational and experimental reports provide somewhat contradictory conclusions. First-principles density functional theory (DFT) calculations predicted ferromagnetic (FM) behavior of Ni-MOF-74[34] while another study gave that Ni-MOF-74 should be antiferromagnetic (AFM) in the ground state.[35] Canepa *et al.* calculated that Ni-MOF-74 should be described as linear ferromagnet with the weak AFM interaction among chains.[36] Rubio-Giménez *et al.* measured temperature- and field dependence of magnetization and concluded qualitatively that Ni-MOF-74 could be described as a combination of weak FM intrachain and weaker AFM interchain interaction.[37] However, recently Son *et al.*[38] reported that Ni-MOF-74 is described as AFM chain with $J \approx -4$ cm^{-1}. Due to many inconsistent results, it seemed necessary to investigate in more detail the magnetic properties of this prototypical MOF.

Herein, we have re-examined the local spin structure and total magnetization of pristine crystalline Ni-MOF-74, with and without solvent molecules populating the voids (*deh*-Ni-MOF-74), using magnetization, X-band electron spin resonance (ESR), multi-frequency high-field ESR (HF-ESR) and theoretical studies. Furthermore, we characterized also 1:1 (Ni:ligand) non-porous coordination polymer that appears as an intermediate during the synthesis of Ni-MOF-74 (Fig. 1d).[39] We were, however, more focused here on the response of Ni-MOF-74 to mechanical stress and the correlation between the electronic structure and magnetic properties of Ni-MOF-74 material depending on the level of internal crystal structure ordering. We found that evacuated Ni-MOF-74 collapses rapidly under mechanical stress imposed by ball-milling, producing stable mechanochemically-induced amorphous phase *am*-Ni-MOF-74. The course of mechanochemical amorphization was directly monitored by *in situ* synchrotron powder X-ray diffraction (PXRD) in tandem with Raman spectroscopy.[40] The collapse of the structure proved to have a strong and profound effect on the electronic structure of Ni(II) nodes, and therefore also on the bulk magnetic properties of amorphous MOF-structure. The observed substantial differences in bulk magnetization between the crystalline and amorphous Ni-MOF-74 were rationalized by insights into the coordination sphere of the metal node acquired by solid-state nuclear magnetic resonance (NMR) and infrared (IR) spectroscopy.

2 Results and discussion

2.1 Synthesis and mechanical processing

We prepared pristine pale-yellow Ni-MOF-74 of general formula $[Ni_2(dhta)(H_2O)_2]\cdot 8H_2O$ from water, following the original re-

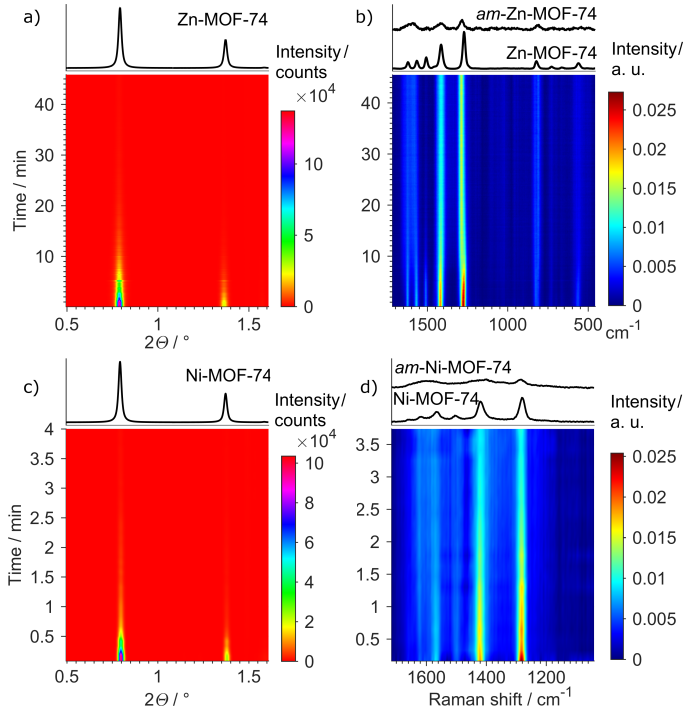

Fig. 2 Tandem *in situ* monitoring data of mechanochemical amorphization of *deh*-Zn-MOF-74 by a) PXRD and b) Raman spectroscopy. Tandem *in situ* monitoring data of mechanochemical amorphization of *deh*-Ni-MOF-74 by c) PXRD and d) Raman spectroscopy.

port from 2006.[32] When the synthesis was performed in 1:1 nickel:ligand ratio and without heating, we were able to isolate $[Ni(dhta)(H_2O)_4]\cdot 2H_2O$ coordination polymer (Ni-INT), which was recently detected and characterized as an intermediate for the mechanochemical preparation of mixed-metal MOF-74 materials.[39] Both products are highly crystalline, as could be seen in Electronic Supplementary Information (ESI) Fig. S1, and benchstable for months. To remove the water molecules from the channels and prepare solvent-free Ni-MOF-74 (*deh*-Ni-MOF-74), we have held pristine Ni-MOF-74, $[Ni_2(dhta)(H_2O)_2]\cdot 8H_2O$, in a vacuum-oven at 90°C for 24 hours. Scanning electron microscopy (SEM) and powder X-ray diffraction (PXRD) showed this sample to remain crystallinity and morphology of the pristine Ni-MOF-74 (Figs. S3 and S2). This dehydrated product was prepared in order to see how the lack of the guests in the MOF structure influence the spin-spin interactions among the nickel centers. *deh*-Ni-MOF-74 was used as a reactant for the mechanochemical amorphization, since the pristine Ni-MOF-74, with water in the channels, remains crystalline after 24 hours milling.

90 minutes of milling of *deh*-Ni-MOF-74 in a ball mill (ESI) afforded dark-brown product without Bragg reflections in PXRD (Fig. S2). We monitored the course of mechanochemical amorphization of *deh*-Ni-MOF-74 by *in situ* synchrotron PXRD in tandem[40] with Raman spectroscopy[41] and compared it to Zn-MOF-74, (Fig. 1c), which was previously reported as an amorphous phase prepared by milling for MOF-alloying purposes.[42] The amorphization is much faster than anticipated; the peaks of MOF-74 start to diminish instantly, and the milled mixture does not show any Bragg reflections after 7 minutes milling for *deh*-Zn-MOF-74, and 3 minutes milling for *deh*-Ni-MOF-74 (Figs. 2a and c). Interestingly, the amorphization induced the changes at molecular level also, clearly seen in Zn-MOF-74 milling experiment as new bands at 1507 and 1622 cm^{-1} in the Raman spectra that grow simultaneously with the loss of crystallinity of the sample (Fig. 2b). In Ni-MOF-74, *in situ* Raman spectra gave much more ambiguous information due to weak luminescence of the sample and broadening of the Raman bands (Fig. 2d). By using PXRD and Raman techniques in tandem, we have not observed any crystalline or non-crystalline intermediates in the monitored experiments.

2.2 Magnetization and ESR study of intermediate complex Ni-INT

We initiated the magnetic study with Ni-INT complex, whose structure is shown in Fig. 1d. The field dependence of magnetization $M(H)$ given in Fig. S4 shows a saturation of magnetization above 6 T with a magnetic moment of about 2.2 μ_B/F.U. (μ_B is the Bohr magneton, F.U. = formula unit) that corresponds to one nickel(II) ion in the unit cell with spin $S = 1$ and g-value of 2.2. Ni-INT complex shows paramagnetic behaviour, as could be seen from temperature dependence of magnetic susceptibility $\chi(T)$ shown in Fig. S5, where fitting to Curie-Weiss law gives Curie temperature $\theta \approx 0$.

As systems with integer-spin ground states $S = 1$ (non-Kramers systems), Ni(II) complexes are usually X- and Q-band ESR silent.[43–46] However, in some particular cases, such as for high symmetry environment around Ni(II) ion, it is possible to detect X-band ESR signal. Fig. S6 shows temperature dependence of X-band ESR spectra of Ni-INT complex. Intensity of spectra grows with lowering the temperature but this dependence shows some deviation from paramagnetic behavior at low temperatures, as could be noticed from the spectral intensities. Furthermore, the HF-ESR spectra show additional lines compared with the spectra of isolated Ni(II) centers with spin $S = 1$,[47] as could be seen from Fig. 3a where selected spectra, together with frequency *vs* resonant magnetic field diagram are shown. The obtained spectra were simulated, using the procedure given in ESI. Temperature dependence of spectra, as well as simulated spectra, are shown in Fig. 3b and good agreement between simulation and experiment could be noticed. The selected simulated X-band spectrum using the same parameters as for HF-ESR spectra is shown in Fig. S6.

Ni-INT has zig-zag chain structure, as it is shown in Fig. 1d. Magnetization results do not support magnetic chain structure but correspond well with paramagnetic non-interacting Ni(II) ions, in line with the large nickel separation in the chains (*ca.* 11.3 Å, Fig. 1d). ESR spectra, however, revealed a certain spin-spin interaction in the Ni-INT complex. The model described by spin-Hamiltonian (S1) in ESI (Section S2, Simulation of ESR spectra of Ni-INT) that includes spin-spin term (S4) results in a good agreement with experimental spectra, in particular in simulation of peaks with $g_2 \approx 3.893$ and $g_5 \approx 2.162$ shown in Fig. 3. The obtained small negative value of exchange parameter J ($|J| < 0.7$ cm^{-1}) points to weak AFM interaction between Ni(II) ions, which was not observed in the less-sensitive magnetization

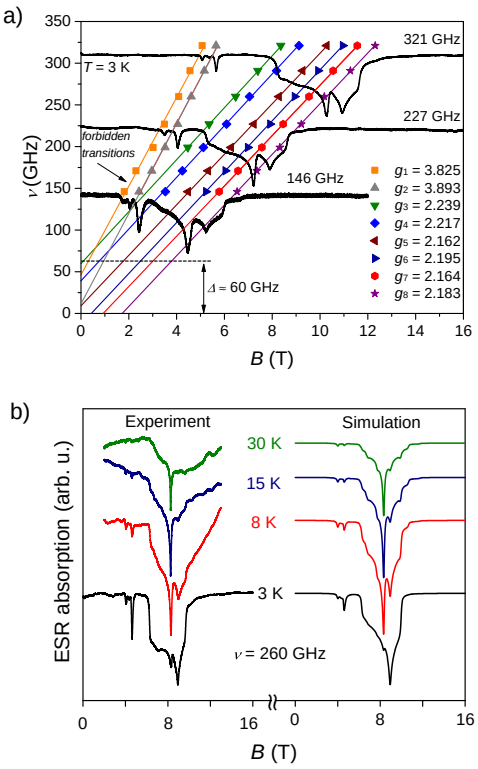

Fig. 3 a) Frequency *vs* resonance field dependencies $\nu(B)$ of the prominent spectral points, together with three selected spectra of Ni-INT complex recorded at different frequencies at $T = 3$ K. b) Temperature dependencies of experimental and simulated spectra of Ni-INT complex at frequency $\nu = 260$ GHz.

measurements. It should be stressed here that including the spin-spin term (S4) is legitimate only for Ni-Ni dimers which are not obvious inside of a polymeric chain in Ni-INT structure. However, as could be seen from the Fig. 1d, the shortest distance of 5.2 Å is between nickel(II) ions in the neighboring chains connected through a hydrogen-bonded ring accomplished by a pair of O–H...O hydrogen bonds between the coordinated water molecules, and the parameter J given by term (S4) describes inter– rather than intra–chain exchange interaction in Ni-INT complex. Therefore, although crystallographically the Ni-chains are well defined, the description of magnetic properties in terms of isolated Ni-dimers with a weak AFM coupling appears to be more appropriate.

2.3 Magnetization study of Ni-MOF-74 derivatives

Temperature dependence The magnetic susceptibilities of Ni-MOF-74, *deh*-Ni-MOF-74 and *am*-Ni-MOF-74 were measured in the temperature range from 1.8 to 300 K. The temperature dependence of $\chi \cdot T$ for all three samples is shown in Fig. 4a. At high temperatures $\chi \cdot T$ saturates to values of 1.3, 1.17 and 0.76 emu K/mol Ni for Ni-MOF-74, *deh*-Ni-MOF-74 and *am*-Ni-MOF-74, respectively. Already from the $\chi \cdot T$ vs. T plot it could be seen that the Ni-MOF-74 and *deh*-Ni-MOF-74 show very similar behavior, while *am*-Ni-MOF-74 is different. For all three samples the spin-only susceptibility was obtained by subtracting the diamagnetic contribution.[48] The obtained χ_{spin} was then fitted to the Curie-Weiss law and the results are summarized in Table 1.

Table 1 Parameters obtained from the fit of spin-only susceptibility to Curie-Weiss law and Néel temperature T_N obtained from the first derivative of the susceptibility

	χ_{dia}[48] (emu/mol)	μ_{eff} (μ_B)	Θ_{CW} (K)	T_N (K)
Ni-MOF-74	$-2.388 \cdot 10^{-4}$	3.1896(2)	+13.55(4)	16.8
deh-Ni-MOF-74	$-1.438 \cdot 10^{-4}$	2.9908(2)	+17.17(2)	15
am-Ni-MOF-74	$-2.388 \cdot 10^{-4}$	2.5803(5)	-15.0(1)	-

The values of effective magnetic moment obtained for Ni-MOF-74 and *deh*-Ni-MOF-74 are within the range expected for Ni(II) high-spin $S = 1$ state,[49] although smaller value is observed for the dehydrated sample. If spin-only angular momentum is assumed for Ni-MOF-74, we obtain $g = 2.26$, which is very similar to the approximate value of 2.24 obtained from HF-ESR study. The same assumption for the dehydrated *deh*-Ni-MOF-74 sample gives a somewhat smaller value of $g = 2.11$, while HF-ESR gives similar approximate value of 2.14. For both samples the positive Curie temperature is observed amounting to ≈ 13 K and ≈ 17 K for Ni-MOF-74 and the *deh*-Ni-MOF-74, respectively. This suggests that dominant interaction between spins is FM for both crystalline MOF-74 materials, irrelevant on the presence of guests in the voids. Furthermore, both samples exhibit a kink in susceptibility corresponding to the phase transition to long-range AFM order (LRAFMO) at Néel temperatures $T_N = 16.8$ K and $T_N = 15$ K for Ni-MOF-74 and the dehydrated sample, respectively (see top and bottom panels of Fig. 4c). This is in agreement with the picture of spin chains with FM intrachain and AFM interchain interaction.[36,37] The phase transition to LRAFMO is also corroborated by the results of X-band ESR experiment. Similar phase transitions were observed for Co-MOF-74[29] and Fe-MOF-74[50] compounds but at lower temperature, around 8 K. Below Néel temperature the susceptibility decreases with the temperature decrease, and below ≈ 5 K it saturates, as can be seen in Fig. 4c. The value measured at lowest temperatures for both samples is approximately equal to $2/3$ of the value measured at T_N, which is expected for the susceptibility of antiferromagnet measured on powder sample.[51] The absence of the low-temperature upturn confirms that there are no paramagnetic impurities in these samples.

Field dependence At temperatures below T_N a metamagnetic phase transition is observed in $M(H)$ curves at ≈ 5.5 T and ≈ 4 T for Ni-MOF-74 and *deh*-Ni-MOF-74, respectively, as can be seen for $T = 1.8$ K in Fig. 4b. Considering the antiferromagnetically ordered ground state at $T = 1.8$ K in both compounds, the observed transition most likely corresponds to field-induced reorientation of spins known as *spin-flop*.[52,53] Spin-flop transition in antiferromagnets occurs in applied magnetic field when the spins rotate from the easy-axis direction to the direction perpendicular to the magnetic field in order to minimize the total energy. A finite value of magnetic field, called spin-flop field, is necessary for Zeeman energy to overcome the anisotropy energy which keeps the spins oriented along the specific crystallographic direction known as easy-axis direction.[52,53] In powder samples this phase transition is, however, usually smeared over finite field range, similar to

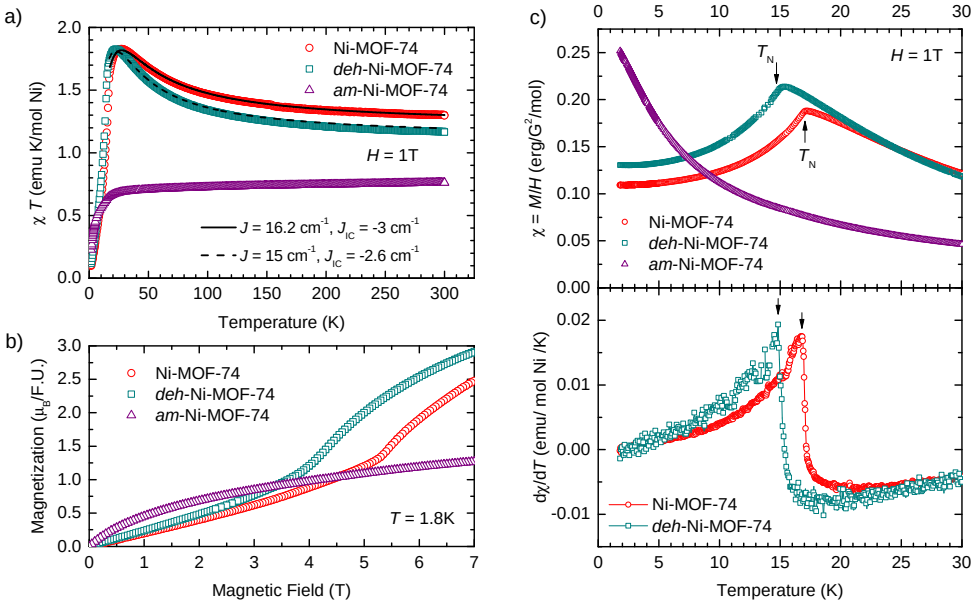

Fig. 4 a) Temperature dependence of χT measured for Ni-MOF-74, dehydrated and amorphous sample. Solid and dashed line represent fit to susceptibility calculated from Fisher's model for $S = 1$ linear chain with intrachain interaction J including the interchain interaction J_{IC} (see text for details). b) Dependence of magnetization on magnetic field measured at $T = 1.8$ K. c) Top panel: low-temperature behavior of magnetic susceptibility for the three samples. Bottom panel: Derivative of susceptibility obtained from measured data for Ni-MOF-74 and dehydrated sample.

what is observed in Fig. 4b. The absence of hysteresis in measured $M(H)$ curves shown in Figs. 4b and 5b for both Ni-MOF-74 and *deh*-Ni-MOF-74 further corroborates this scenario, as well as the fact that for those two samples at maximum measured field of 7 T, the saturation of magnetization is not reached; the values of 2.5 and 3 μ_B/F.U. are far below the value of 4.4 μ_B/F.U expected for two Ni(II) spins. This points at the significance of the AFM interaction which cannot be overcome by the highest applied magnetic field of 7 T. The spin-flop phase transition for Ni-MOF-74 is observed also at $T = 10$ K but at lower field compared to $\mu_0 H \approx 5.5$ T obtained at 1.8 K (Fig. 5b). This transition disappears with increasing the temperature around 15 K, as the compound is no longer in antiferromagnetically ordered state. The similar temperature dependence of susceptibility with $T_N = 16.8$ K is observed also in lower magnetic field of 0.1 T, as can be seen in Fig. 5a for Ni-MOF-74. However, in strong magnetic field of 7 T (Fig. 5a), the susceptibility displays temperature behavior typical for susceptibility measured along the hard axis of antiferromagnet.[54] This is in agreement with our proposition that the spin-flop transition occurs at $\mu_0 H \approx 5.5$ T; at larger magnetic field all the spins will be perpendicular to applied magnetic field and hard-axis susceptibility will be measured. While similar metamagnetic spin-flop behaviour was observed for Co-MOF-74,[29] the hysteresis was recorded in $M(H)$ curves for this sample.[29] On the contrary, the hysteresis was not observed for Fe-MOF-74,[50] revealing significantly different magnetic picture of these otherwise similar compounds.

Amorphous sample *am*-Ni-MOF-74 displays different behavior than Ni-MOF-74 and *deh*-Ni-MOF-74, as can be seen in Fig. 4. The results obtained from the fit to the Curie-Weiss law (Table 1) show that the value of effective magnetic moment is much smaller for amorphous sample, and significantly diverging from the values expected for high-spin Ni(II) with $S = 1$. If spin-only angular momentum is assumed, the value of g-factor obtained from the Curie constant, assuming Ni(II) carries spin $S = 1$, amounts to nonphysical value $g = 1.8$, indicating that the certain amount of spins are missing. Since nickel is not lost during the amorphization procedure, it is reasonable to assume that part of Ni(II) have turned to the low-spin $S = 0$ state. This is possible if the coordination sphere of the Ni(II) has changed from octahedral to square-planar,[49,55,56] trigonal-bipyramidal[57–59] or square-pyramidal[60,61] configuration. At low temperatures the susceptibility of the amorphous sample increases with the temperature decrease, following a Curie-Weiss law with negative $\Theta = -15$ K, signifying that AFM interactions are dominant. Phase transition to long-range magnetic order is not observed in this sample (Fig. 4c). The field-dependence of magnetization is shown in Fig. 4b. As the field increases the magnetization first increases rapidly and then slowly saturates towards a value which is much smaller than the saturation value expected for two high-spin Ni(II) per formula unit, and which is expected to be reached for paramagnetic spins $S = 1$ in applied magnetic field and temperature. This further corroborates the partial lack of $S = 1$ sites (approximately half) in comparison with Ni-MOF-74 and the dehydrated sample.

2.3.1 Extended Fisher model

Using the previous results, we considered a possible theoretical model to describe the magnetic properties of Ni-MOF-74 and *deh*-Ni-MOF-74. In Ni-MOF-74 structure, nickel(II) nodes interact through super-exchange over oxygen atoms in the chains but also through direct exchange interaction due to the small distances between nearest neighbors (3.0 Å, Fig. 1b). Additionally, there is a

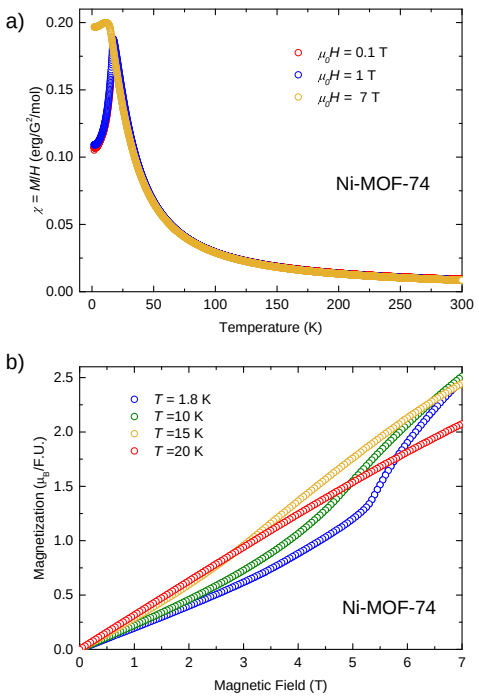

Fig. 5 a) Temperature dependencies of susceptibility χ *vs* T recorded in indicated fields. b) Field dependencies of the magnetization M *vs* H, recorded in two cycles 0–7 T and 7–0 T, at different temperatures.

significant interaction between next-nearest neighbors separated by 4.9 Å. Furthermore, zero-field splitting (ZFS) parameters (for spin of metal ions $S > 1/2$) and inter-chain interactions should be taken into account, making magnetic picture of Ni-MOF-74 even more complicated (Fig. 1b).[36] In order to describe magnetization results, we considered Ni-MOF-74 as chains of Ni(II) ions with the exchange interaction J_{NN} between the nearest-neighbours while the interaction J_{NNN} between next-nearest neighbors is neglected. The closest distance between Ni(II) ions in different chains is 7.4 Å so it could be approximated that interchain interaction J_{IC} is smaller compared to the intrachain. Therefore, we used extended Fisher model with an additional term J_{IC} that accounts for interaction of the chain with neighboring chains.[36,62–64] This is justified since long-range magnetic ordering is observed in these samples confirming the importance of interchain interactions. In Fisher's model magnetic chains are formed through nearest-neighbor isotropic Heisenberg coupling J_{NN} between the spins and the susceptibility is given by:[62,64]

$$\chi_0 = \frac{Ng^2\mu_B^2 S(S+1)}{3k_B T}\frac{1+u(J_{NN})}{1-u(J_{NN})}, \quad (1)$$

with

$$u(J_{NN}) = coth(\frac{J_{NN}S(S+1)}{k_B T}) - \frac{k_B T}{J_{NN}S(S+1)}, \quad (2)$$

where $S = 1$ and $g = 2.2$ for nickel ions, and the constant k_B is the Boltzmann constant. In extended Fisher model with the term that includes interaction of the chain with $z = 3$ other neighbouring chains in the molecular field approximation, the derived expression for the temperature dependence of magnetic susceptibility is:[65]

$$\chi = \frac{\chi_0}{1 - \frac{zk_B J_{IC}}{Ng^2\mu_B^2}\chi_0}. \quad (3)$$

The corresponding fits for Ni-MOF-74 and *deh*-Ni-MOF-74 based on Eq. 1–3 are plotted in Fig. 4a by solid and dashed lines, respectively. The obtained values of intrachain and interchain interactions are: $J_{NN} = 16.2$ cm^{-1}, $J_{IC} = -3$ cm^{-1} and $J_{NN} = 15$ cm^{-1}, $J_{IC} = -2.6$ cm^{-1}, for Ni-MOF-74 and *deh*-Ni-MOF-74, respectively. It should be mentioned that fits are used only for data with $T > T_N$ (above 18 and 16 K, for Ni-MOF and *deh*-Ni-MOF-74, respectively). This model shows quite good agreement with the experimental data, revealing that the assumption about weak FM intrachain and weaker AFM interchain interaction in Ni-MOF-74 is reasonable. However, despite the good agreement of the used theoretical model with the observed experimental data, we stress that the obtained value of $J_{IC} = -3$ cm^{-1}(-4.3 K) is small to account for AFM ordering at Néel temperature of 17 K in Ni-MOF-74. This result suggests that even more complicated magnetic interaction paths, such as neglected interaction J_{NNN} between next-nearest neighbors, need to be considered to fully capture the magnetism of the Ni-MOF-74 compound.

2.4 ESR spectroscopy of Ni-MOF-74 derivatives

To gain an insight into the local magnetic properties of Ni-MOF-74 derivatives, we employed X-band- and multi-frequency HF-ESR spectroscopy. Above 15.8 K and 15 K for Ni-MOF-74 and *deh*-Ni-MOF-74, respectively, very broad ESR line is detected (spectra shown in color) while below these temperatures, ESR lines disappear, pointing to the magnetic ordering in these compounds, Fig. 6a. These temperatures are in very good agreement with Néel temperatures obtained from magnetization measurements given in Table 1 in the previous section. *am*-Ni-MOF-74 sample was X-band ESR silent; only small peak at $g = 2.00$ was detected revealing that during amorphization process small amount of free radicals was produced.

Temperature dependencies of HF-ESR spectra of Ni-MOF-74, *deh*-Ni-MOF-74 and *am*-Ni-MOF-74 are presented in Fig. 6b and it could be noticed that the spectra in the whole temperature range are observed, even below the Néel temperatures. *am*-Ni-MOF-74 shows HF-ESR signal but with significantly lower intensity compared to other two samples, Fig. S7. However, in contrast to the HF-ESR spectra recorded in the paramagnetic regime at elevated temperature, the spectra obtained in the magnetically ordered state at $T < T_N$ display AFM collective resonance modes and not paramagnetic signals. This effect is particularly evident in the observation of additional lines in the magnetic field region around 5.5 and 4 T for Ni-MOF-74 and *deh*-Ni-MOF-74, respectively (see the spectra at 10 K in Fig. 6b, which is in line with spin-flop transition observed in $M(H)$-curves at the same magnetic field values (Fig. 4b and 5b). Therefore, the spectra at temperatures higher than Néel temperatures should be used to get the information for the compounds in the paramagnetic state. The selected spectra of Ni-MOF-74, *deh*-Ni-MOF-74 and *am*-Ni-MOF-74 compounds together with ν vs B dependence at $T = 60$ K are shown in Fig. S8. From the graphs, it is possible to obtain approximate

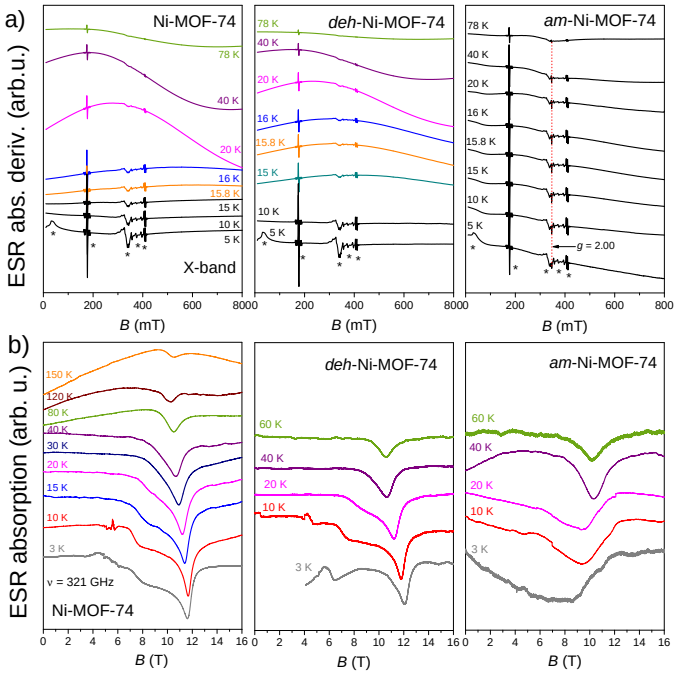

Fig. 6 a) Temperature dependence of X-band ESR spectra of Ni-MOF-74, *deh*-Ni-MOF-74 and *am*-Ni-MOF-74 compounds. Sharp peaks marked by asterisks are the cavity signals. The line with $g = 2.00$ (dashed vertical line) points to the presence of free radicals in *am*-Ni-MOF-74. b) Temperature dependencies of HF-ESR spectra of Ni-MOF-74, *deh*-Ni-MOF-74 and *am*-Ni-MOF-74 compounds at frequency $\nu = 321$ GHz.

values of g-factor: $g \approx 2.24$, 2.14 and 2.36 for Ni-MOF-74, *deh*-Ni-MOF-74 and *am*-Ni-MOF-74, respectively. To obtain more accurate values of g-values and other spin-Hamiltonian parameters, it is necessary to perform spectral simulation.[66–68] However, due to large number of interactions (ZFS, intrachain and interchain exchange interactions) and related parameters that have to be included into the simulations on the one side, and rather featureless high-temperature ESR spectra on the other side, the results of such simulations would be rather ambiguous. Nevertheless, on the qualitative level, from the Fig. 6 and Fig. S8, one can see that line-width and shape for Ni-MOF-74 and *deh*-Ni-MOF-74 are similar and therefore, we can conclude that in desolvation process the nickel coordination sphere stayed approximately unchanged. Absence of the X-band signal of *am*-Ni-MOF-74 sample as well as broader HF-ESR line-widths with significantly lower intensity, are in agreement with the assumption that some amount of paramagnetic Ni(II) ions with $S = 1$ obey transition into the nonmagnetic $S = 0$ state while the ESR signal of remaining nickel ions with $S = 1$ is smaller in amplitude due to amorphization and line broadening.

2.5 Solid state NMR spectroscopy of Ni-MOF-74 derivatives

We attempted to obtain additional insight into the local structure of Ni-MOF-74, *deh*-Ni-MOF-74 and *am*-Ni-MOF-74 by measuring ^{13}C MAS NMR spectra of these materials. ^{13}C nuclei are sensitive probes of local magnetic fields and are vastly exploited in NMR spectroscopy of diamagnetic carbon-containing materials, where their spectra offer information about the details of their local environments. For ferro-, antiferro- and paramagnetic materials ^{13}C NMR spectra are typically not easy to understand. Unlike for diamagnetic materials, the shifts observed in the spectra of magnetic materials are difficult to predict, because they predominantly depend on the hyperfine interaction of ^{13}C nuclei with the spins of the unpaired electrons, and can vary drastically depending on the distances between the nuclei and the electronic spins and on the magnitude and sign of the contact (Fermi) hyperfine coupling constant. Only recently, first attempts of calculating such shifts in paramagnetic MOFs have emerged.[69–71]

The ^{13}C MAS NMR spectra of Ni-MOF-74, *deh*-Ni-MOF-74 and *am*-Ni-MOF-74 are shown in Fig. 7. ^{13}C MAS NMR spectra of Ni-MOF-74 and *deh*-Ni-MOF-74 differ mainly in the widths of individual signals. Although ^{13}C MAS NMR spectrum of Ni-MOF-74 exhibits a large number of resonance lines in a very wide range between 2000 and -800 ppm, it can be decomposed into only seven spinning sideband patterns (Fig. S9). Broad spinning sideband patterns, shifted for several hundred or even thousand ppm from the region of typical chemical shifts, are a fingerprint of a strong interaction of ^{13}C nuclei with the electronic spins. A closer look at the spectrum tells us that the seven sideband patterns actually belong to four significantly different types of carbon atoms, characterized by isotropic shifts of about 240, 850, 910 and 1220 ppm and by equal abundances. Three of these four contributions actually comprise two sideband patterns, one with rather narrow signals and another with broader signals, but with almost the same isotropic shift and with the same shape of the spinning sideband pattern. This duality suggests that the pristine Ni-MOF-74, used in the NMR analysis, might not be entirely homogeneous. It is possible that part of the sample is better crystalline and thus gives rise to narrower signals, and part is of poorer crystallinity, giving rise to broader signals (very similar to those observed in *deh*-Ni-MOF-74). Another possible explanation could also be a varying degree of hydration throughout the crystalline framework of pristine Ni-MOF-74.

The ^{13}C MAS NMR spectrum of *am*-Ni-MOF-74 comprises three types of signals (Fig. 7). Very sharp signals at 18, 45, 52, and 178 ppm probably belong to polymethyl-methacrylate (PMMA) impurity from the milling vessels. These signals represent only about 5% of the total signal intensity and can be detected also in the spectra of Zn-MOF-74 and *am*-Zn-MOF-74 (Fig. S10). More than 80% of the intensity is in the very broad Gaussian-shaped signal extending between -400 and 1400 ppm. This signal undoubtedly belongs to the amorphous phase. The signals of the third type are weak and moderately broadened. Isotropic shifts of 213 and 128 ppm, which only slightly deviate from chemical shifts typical for diamagnetic ligands, indicate the presence of a weak interaction with paramagnetic centers. These signals could be assigned to radicals, small concentration of which was detected within this sample by X-band ESR spectroscopy. Altogether, the above discussed magnetic properties of Ni-MOF-74, *deh*-Ni-MOF-74 and *am*-Ni-MOF-74 are clearly reflected in the ^{13}C MAS NMR spectra of these materials. However, the NMR spectra also suggest that the samples are somewhat less homogeneous than it was proposed by diffraction.

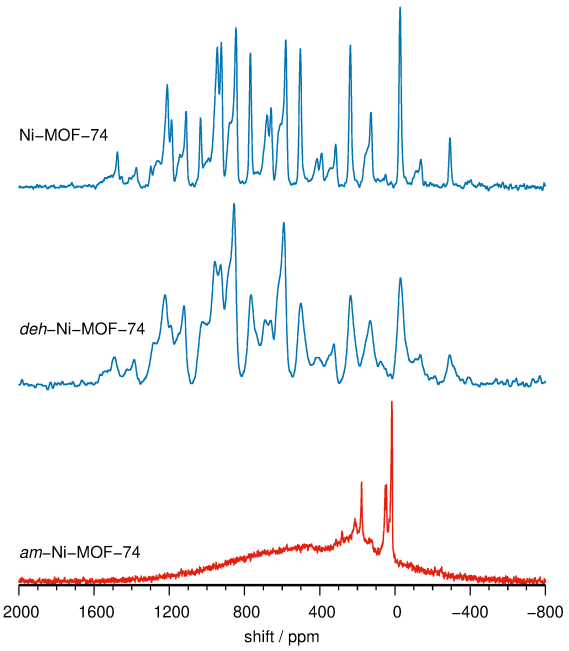

Fig. 7 ^{13}C MAS NMR spectra of Ni-MOF-74, *deh*-Ni-MOF-74 and *am*-Ni-MOF-74.

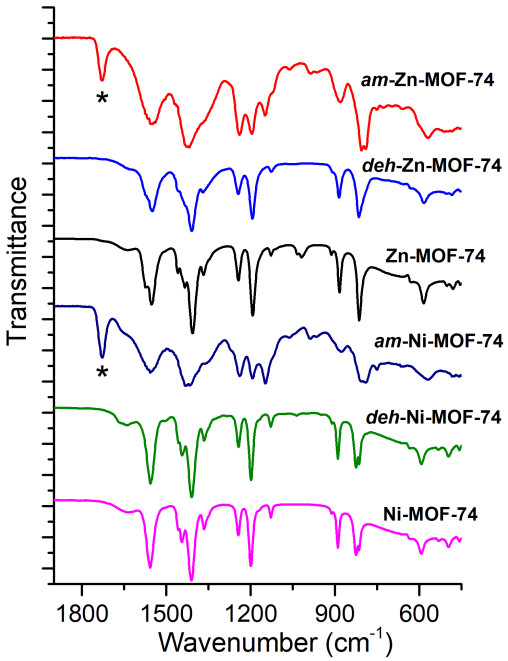

Fig. 8 FTIR-ATR data of Ni-MOF-74 (pink), *deh*-Ni-MOF-74 (green), *am*-Ni-MOF-74 (dark blue), Zn-MOF-74 (black), *deh*-Zn-MOF-74 (blue) and *am*-Zn-MOF-74 (red). The new C=O band (denoted with asterisk) at *ca.* 1728 cm^{-1} is present in both *am*-Ni-MOF-74 and *am*-Zn-MOF-74.

2.6 IR spectroscopy of Ni-MOF-74 derivatives

Fourier-transform infrared attenuated total reflectance spectroscopy (FTIR-ATR) proved particularly useful for corroborating observations from *in situ* Raman data as well as magnetization and ESR study about the potential molecular changes in the ligand occurring during amorphization process. Vibrational spectra of Ni-MOF-74 and *deh*-Ni-MOF-74 compounds are similar, and the *am*-Ni-MOF-74 has very different IR spectrum. Spectrum of Ni-MOF-74 is characterized by strong, sharp and well-defined peaks that broaden and change upon amorphization. The most pronounced difference, however, is a disappearance of a band at 1617 cm^{-1} in Ni-MOF-74 (1622 cm^{-1} in Zn-MOF-74), and appearance of a medium-strong band at 1728 cm^{-1} for *am*-Ni-MOF-74 that may be ascribed to a free carboxyl group (Fig. 8). Formation of C=O group may only be related to breaking of carboxyl-nickel bonds and the alteration of the coordination sphere around metal node with the linkers building the walls characteristic of MOF-74 (Fig. 1b), so we expect for a portion of nickel centers in *am*-Ni-MOF-74 do not have conventional octahedral coordination anymore as in pristine Ni-MOF-74 and *deh*-Ni-MOF-74, with the nickel cation in high-spin d^8 configuration.

2.7 Recrystallization of amorphous MOF-74 materials

In the recent report describing amorphization in several MOFs,[42] authors hypothesized that recrystallization depends on the preservation of the coordination sphere of the metal node, so we used this technique to further assess whether the nickel(II) coordination sphere was "damaged". Thus, we attempted to recrystallize *am*–Ni-MOF-74 sample by aging in suitable atmosphere[72] and by liquid-assisted grinding (LAG)[73] with methanol or water. Unlike Zn-MOF-74, which recrystallize after a short aging in methanol vapors,[42] *am*–Ni-MOF-74 behaves completely different. The MOF-74 structure was not established even after 14 days standing of *am*–Ni-MOF-74 in methanol or water vapors at 45°C (Fig. S14). The aging products display only very weak Bragg reflections at 6.98 and 11.99 2Θ angle, hardly visible in experimental data. *In situ* monitoring confirmed LAG (MeOH or water) procedures to be highly effective for recrystallization of Zn-MOF-74, resulting in a crystalline MOF-74 structure in less than 3 minutes milling (Fig. S12). LAG did not induce crystallization for *am*–Ni-MOF-74 (Fig. S13) despite longer milling times, switching to dimethylformamide additive, or increase in the liquid-additive content. While this further confirms that the nickel(II) coordination sphere is interrupted, it also attracted our attention; Zn-MOF-74 and Ni-MOF-74 have almost identical crystal structures (Fig. 1a) characterized by the same octahedral coordination mode of metal cation; (Fig. 1c) and very similar FTIR upon amorphization. The difference in recrystallization potential implies that the mechanical behavior of MOF-74 will strongly depend on the metal cation building the structure and that more attention needs to be given to the type of the metal in development of applicable MOF-74 materials. This irreversibility may also have strong impact on the potential applicability of amorphous Ni-MOF-74, since the main obstacle for the consideration of amorphous MOFs for device production is the fact they often and readily recrystallize, thus changing their volume and morphology significantly.[23]

3 Conclusions

To summarize, we have used magnetization, X-band and high-field ESR experiments, supported with extended Fisher model, to describe magnetic properties of Ni-MOF-74 with different lev-

els of internal ordering. Our results reveal the magnetism of Ni-MOF-74 to be dominated by ferromagnetic exchange interaction ($J \approx 16$ cm^{-1}) in the helical nickel-oxo chains and weaker antiferromagnetic interaction ($J \approx -3$ cm^{-1}) between the adjacent chains. Furthermore, the results showed long-range AFM phase transition at $T_N = 16.8$ K and metamagnetic spin-flop behavior in Ni-MOF-74. The removal of the solvent molecules from the Ni-MOF-74 channels does not influence the magnetic properties of the Ni-MOF-74 material significantly. Contrary to the desolvation, the amorphization process has a profound influence on physical properties of Ni-MOF-74, resulting in a significant decrease of the bulk magnetization in *am*-Ni-MOF-74. The results of spectroscopic studies indicate that this decrease is directly related to changes of the coordination sphere of the metal center occurring upon mechanical action, resulting in the spin-crossover from the magnetic high-spin state with $S = 1$ to non-magnetic low-spin state with $S = 0$. From the magnetic susceptibility measurements for *am*-Ni-MOF-74 we conclude that not all nickel centers are subject to the spin-crossover, around half of them are in the high-spin $S = 1$ state while the rest are in the low-spin $S = 0$ state. The amorphization of Ni-MOF-74 is irreversible (almost unchanged after different LAG experiments and weeks of aging in various atmospheres), whereas isostructural Zn-MOF-74, showing similar vibrational spectra after amorphization, recrystallizes readily in aging or LAG procedures. This difference reveals the profound influence of metal cation on net stability, which needs to be taken into account in developing application of amorphous MOF-74 materials.

Conflicts of interest

There are no conflicts to declare.

Acknowledgements

We thank Dr. A. Alfonsov and Dr. A. Popov from Leibniz IFW Dresden for help with HF-ESR measurements and for preparing *deh*-Ni-MOF-74, respectively and also Prof. M. Ilakovac Kveder for useful NMR discussion. We thank to Dr. M. di Michiel and beamline ID-15 at the European Synchrotron Radiation Facility for the collection of in-situ monitoring data. The authors acknowledge the Croatian Science Foundation (CSF) (grant nos. UIP-2014-09-4744 and IP-2018-01-3168) for financial support, CSF and the European Social Fund for support through grant PZS-2019-02-4129), and German (DAAD)-Croatian (MZO) bilateral project: *Magneto-structural correlations in molecular magnetic complexes studied by electron spin resonance spectroscopy*. GM acknowledges financial support from the Slovenian Research Agency (research core funding No. P1-0021 and project No. N1-0079).

Notes and references

1 M. O. H. Li, M. Eddaoudi and O. M. Yaghi, *Nature*, 1999, 276.
2 G. Férey, *Chem. Soc. Rev.*, 2008, **37**, 191.
3 S. Yuan, L. Feng, K. Wang, J. Pang, M. Bosch, C. Lollar, Y. Sun, J. Qin, X. Yang, P. Zhang, Q. Wang, L. Zou, Y. Zhang, L. Zhang, Y. Fang, J. Li and H.-C. Zhou, *Adv. Mater.*, 2018, **30**, 1704303.
4 S. Ma and H.-C. Zhou, *Chem. Commun.*, 2010, **46**, 44.
5 A. E. Baumann, D. A. Burns, B. Liu and V. S. Thoi, *Commun. Chem.*, 2019, **2**, 86.
6 J.-R. Li, J. Sculley and H.-C. Zhou, *Chem. Rev.*, 2012, **112**, 869.
7 Z. R. Herm, E. D. Bloch and J. R. Long, *Chem. Mater.*, 2014, **26**, 323.
8 R.-B. Lin, S. Xiang, H. Xing, W. Zhou and B. Chen, *Coord. Chem. Rev.*, 2019, **378**, 87.
9 C. Y. Lee, O. K. Farha, B. J. Hong, A. A. Sarjeant, S. T. Nguyen and J. T. Hupp, *J. Am. Chem. Soc.*, 2011, **133**, 15858.
10 M. C. So, G. P. Wiederrecht, J. E. Mondloch, J. T. Hupp and O. K. Farha, *Chem. Commun.*, 2015, **51**, 3501.
11 M. J. Kalmutzki, C. S. Diercks and O. M. Yaghi, *Adv. Mater.*, 2018, **30**, 1704304.
12 L. E. Kreno, K. Leong, O. K. Farha, M. Allendorf, R. P. Van Duyne and J. T. Hupp, *Chem. Rev.*, 2012, **112**, 1105.
13 Y. Liu, X.-Y. Xie, C. Cheng, Z.-S. Shao and H.-S. Wang, *J. Mater. Chem. C*, 2019, **7**, 10743.
14 N. S. Bobbitt, M. L. Mendonca, A. J. Howarth, T. Islamoglu, J. T. Hupp, O. K. Farha and R. Q. Snurr, *Chem. Soc. Rev.*, 2017, **46**, 3357.
15 J. E. Mondloch, M. J. Katz, W. C. I. III, P. Ghosh, P. Liao, W. Bury, G. W. Wagner, M. G. Hall, J. B. DeCoste, G. W. Peterson, R. Q. Snurr, C. J. Cramer, J. T. Hupp and O. K. Farha, *Nat. Mater.*, 2015, **14**, 512.
16 L. Zhu, X.-Q. Liu, H.-L. Jiang and L.-B. Sun, *Chem. Rev.*, 2017, **117**, 8129.
17 A. Dhakshinamoorthy, Z. Li and H. Garcia, *Chem. Soc. Rev.*, 2018, **47**, 8134.
18 J. Lee, O. K. Farha, J. Roberts, K. A. Scheidt, S. T. Nguyen and J. T. Hupp, *Chem. Soc. Rev.*, 2009, **38**, 1450.
19 F.-X. Coudert, *Chem. Mater.*, 2015, **27**, 1905.
20 E. Coronado and G. Minguez Espallargas, *Chem. Soc. Rev.*, 2013, **42**, 1525.
21 L. R. Redfern and O. K. Farha, *Chem. Sci.*, 2019, **10**, 10666.
22 S. Chibani and F.-X. Coudert, *Chem. Sci.*, 2019, **10**, 8589.
23 N. C. Burtch, J. Heinen, T. D. Bennett, D. Dubbeldam and M. D. Allendorf, *Adv. Mater.*, 2018, **30**, 1704124.
24 T. D. Bennett and A. K. Cheetham, *Acc. Chem. Res.*, 2014, **47**, 1555.
25 T. D. Bennett and S. Horike, *Nat. Rev. Mater.*, 2018, **3**, 431.
26 J. M. Tuffnell, C. W. Ashling, J. Hou, S. Li, L. Longley, M. L. Ríos Gómez and T. D. Bennett, *Chem. Commun.*, 2019, **55**, 8705.
27 A. M. Sheveleva, D. I. Kolokolov, A. A. Gabrienko, A. G. Stepanov, S. A. Gromilov, I. K. Shundrina, R. Z. Sagdeev, M. V. Fedin and E. G. Bagryanskaya, *J. Phys. Chem. Lett.*, 2014, **5**, 20.
28 N. L. Rosi, J. Kim, M. Eddaoudi, B. Chen, M. O'Keeffe and O. M. Yaghi, *J. Am. Chem. Soc.*, 2005, **127**, 1504.
29 P. D. C. Dietzel, Y. Morita, R. Blom and H. Fjellvåg, *Angew. Chem. Int. Ed.*, 2005, **44**, 6354.
30 M. T. Kapelewski, S. J. Geier, M. R. Hudson, D. Stük, J. A. Mason, J. N. Nelson, D. J. Xiao, Z. Hulvey, E. Gilmour, S. A.

FitzGerald, M. Head-Gordon, C. M. Brown and J. R. Long, *J. Am. Chem. Soc.*, 2014, **136**, 12119.
31 S. Han, H. Kim, J. Kim and Y. Jung, *Phys. Chem. Chem. Phys.*, 2015, **17**, 16977.
32 P. D. C. Dietzel, B. Panella, M. Hirscher, R. Blom and H. Fjellvåg, *Chem. Commun.*, 2006, 959.
33 C. M. Brown, A. J. Ramirez-Cuesta, J.-H. Her, P. S. Wheatley and R. E. Morris, *Chem. Phys.*, 2013, **427**, 3.
34 Q. Zhang, B. Li and L. Chen, *Inorg. Chem.*, 2013, **52**, 9356.
35 D. Yu, A. O. Yazaydin, J. R. Lane, P. D. C. Dietzel and R. Q. Snurr, *Chem. Sci.*, 2013, **4**, 3544.
36 P. Canepa, Y. J. Chabal and T. Thonhauser, *Phys. Rev. B*, 2013, **87**, 094407.
37 V. Rubio-Giménez, J. C. Waerenborgh, J. M. Clemente-Juan and C. Martí-Gastaldo, *Chem. Mater.*, 2017, **29**, 6181.
38 K. Son, J. Y. Kim, G. Schütz, S. G. Kang, H. R. Moon and H. Oh, *Inorg. Chem.*, 2019, **58**, 8895.
39 G. Ayoub, B. Karadeniz, A. J. Howarth, O. K. Farha, I. Đilović, L. S. Germann, R. E. Dinnebier, K. Užarević and T. Friščić, *Chem. Mater.*, 2019, **31**, 5494.
40 S. Lukin, T. Stolar, M. Tireli, M. V. Blanco, D. Babić, T. Friščić, K. Užarević and I. Halasz, *Chem. Eur. J.*, 2017, **23**, 13941.
41 D. Gracin, V. Štrukil, T. Friščić, I. Halasz and K. Užarević, *Angew. Chem. Int. Ed.*, 2014, **53**, 6193.
42 T. Panda, S. Horike, K. Hagi, N. Ogiwara, K. Kadota, T. Itakura, M. Tsujimoto and S. Kitagawa, *Angew. Chem. Int. Ed.*, 2017, **56**, 2413.
43 J. Krzystek, J.-H. Park, M. W. Meisel, M. A. Hitchman, H. Stratemeier, L.-C. Brunel and J. Telser, *Inorg. Chem.*, 2002, **41**, 4478.
44 M. Jurić, P. Planinić, D. Žilić, B. Rakvin, B. Prugovečki and D. Matković-Čalogović, *J. Mol. Struct.*, 2009, **924-926**, 73.
45 L. Androš Dubraja, K. Molčanov, D. Žilić, B. Kojić-Prodić and E. Wenger, *New J. Chem.*, 2017, **41**, 6785.
46 D. Vušak, N. Smrečki, B. Prugovečki, I. Đilović, I. Kirasić, D. Žilić, S. Muratović and D. Matković-Čalogović, *RSC Adv.*, 2019, **9**, 21637.
47 Y. Krupskaya, A. Alfonsov, A. Parameswaran, V. Kataev, R. Klingeler, G. Steinfeld, N. Beyer, M. Gressenbuch, B. Kersting and B. Büchner, *ChemPhysChem*, 2010, **11**, 1961.
48 G. A. Bain and J. F. Berry, *J. Chem. Educ.*, 2008, **85**, 532.
49 H. L. Schläfer and G. Gliemann, *Basic Principles of Ligand Field Theory*, Wiley-Interscience, New York, 1969.
50 R. Maurice, P. Verma, J. M. Zadrozny, S. Luo, J. Borycz, J. R. Long, D. G. Truhlar and L. Gagliardi, *Inorg. Chem.*, 2013, **52**, 9379.
51 N. A. Spaldin, *Magnetic Materials: Fundamentals and Applications*, Cambridge University Press, Cambridge, 2013.
52 L. Néel, *Proc. Phys. Soc. A*, 1952, **65**, 869.
53 K. Yosida, *Prog. Theor. Phys.*, 1951, **6**, 691.
54 S. Blundell, *Magnetism in Condensed Matter*, Oxford University Press, Oxford, UK, 2006.
55 H. Ohtsu and K. Tanaka, *Chem. Eur. J.*, 2005, **11**, 3420.
56 M. Klaß, J. Krahmer, C. Näther and F. Tuczek, *Dalton Trans.*, 2018, **47**, 1261.
57 O. Headley, R. Nyholm, C. McAuliffe, L. Sindellari, M. Tobe and L. Venanzi, *Inorg. Chim. Acta*, 1970, **4**, 93.
58 J. W. Dawson, H. B. Gray, J. E. Hix, J. R. Preer and L. M. Venanzi, *J. Am. Chem. Soc.*, 1972, **94**, 2979.
59 M. Mathew, G. J. Palenik, G. Dyer and D. W. Meek, *J. Chem. Soc., Chem. Commun.*, 1972, 379.
60 H. B. Gray and J. R. Preer, *J. Am. Chem. Soc.*, 1970, **92**, 7306.
61 A. Bianchi, P. Dapporto, G. Fallani, C. A. Ghilardi and L. Sacconi, *J. Chem. Soc., Dalton Trans.*, 1973, 641.
62 M. E. Fisher, *Am. J. Phys.*, 1964, **32**, 343.
63 E. D. Bloch, W. L. Queen, R. Krishna, J. M. Zadrozny, C. M. Brown and J. R. Long, *Science*, 2012, **335**, 1606.
64 O. Kahn, *Molecular Magnetism*, Wiley-VCH Inc., 1993.
65 R. L. Carlin and A. J. Van Duyneveldt, *Magnetic properties of transition metal compounds*, Springer-Verlag, New York, 1977.
66 D. Žilić, L. Androš, Y. Krupskaya, V. Kataev and B. Büchner, *Appl. Magn. Reson.*, 2015, **46**, 309.
67 D. Žilić, K. Molčanov, M. Jurić, J. Habjanič, B. Rakvin, Y. Krupskaya, V. Kataev, S. Wurmehl and B. Büchner, *Polyhedron*, 2017, **126**, 120.
68 L. Androš, M. Jurić, J. Popović, D. Pajić, Y. Krupskaya, V. Kataev, B. Büchner and D. Žilić, *Dalton Trans.*, 2018, **47**, 3992.
69 T. Wittmann, A. Mondal, C. B. L. Tschense, J. J. Wittmann, O. Klimm, R. Siegel, B. Corzilius, B. Weber, M. Kaupp and J. Senker, *J. Am. Chem. Soc.*, 2018, **140**, 2135.
70 Z. Ke, L. E. Jamieson, D. M. Dawson, S. E. Ashbrook and M. Bühl, *Solid State Nucl. Magn. Reson.*, 2019, **101**, 31.
71 D. M. Dawson, C. E. Sansome, L. N. McHugh, M. J. McPherson, L. J. M. McPherson, R. E. Morris and S. E. Ashbrook, *Solid State Nucl. Magn. Reson.*, 2019, **101**, 44.
72 P. A. Julien, C. Mottillo and T. Friščić, *Green Chem.*, 2017, **19**, 2729.
73 T. Friščić, S. L. Childs, S. A. A. Rizvi and W. Jones, *CrystEngComm*, 2009, **11**, 418.